Supplementary Material

Tidewater glaciers and bedrock characteristics control the phytoplankton growth environment in a fjord in the Arctic

Laura Halbach, Mikko Vihtakari, Pedro Duarte, Alistair Everett, Mats A. Granskog, Haakon Hop, Hanna M. Kauko, Svein Kristiansen, Per I. Myhre, Alexey K. Pavlov, Ankit Pramanik, Agnieszka Tatarek, Tomas Torsvik, Józef M. Wiktor, Anette Wold, Angela Wulff, Harald Steen and Philipp Assmy*

*** Correspondence:** Corresponding Author: philipp.assmy@npolar.no

Supplementary Methods

1.1 Phytoplankton community analysis

Environmental patterns in the phytoplankton community composition were examined using environmental variables fitted on principal component analysis of log +1 transformed species matrix (envfit function from vegan package; Oksanen et al., 2018).

1.2 Modelling of glacier runoff rates

A coupled energy balance – snow/firn model (Van Pelt et al., 2012) was used to simulate discharge from the individual glaciers of the Kongsfjorden basin (Pramanik et al., 2018). The energy balance model simulates surface melt due to all the energy fluxes that the glacier is interacting with. Melt water produced at the surface percolates down the snowpack, where it refreezes and stores depending on the temperature, density, and porosity of the snowpack, and the residual water, if any, runs off at the snow-ice boundary, which finally enters the fjord.

1.3 Modelling of plume entrainment rates

In order to estimate the potential primary production that can be sustained by glacier-induced nutrient upwelling in Kongsfjorden, the entrainment volumes were modelled on the basis of meltwater subglacial discharge rates and plume dynamics at Kronebreen for 2017 (doi/10.5281/zenodo.2198959). As plumes of subglacial discharge rise they entrain ambient water and expand, driving an additional source of upwelling within the fjord. To estimate the volume of upwelling driven by subglacial discharge plumes, we implemented a simple plume model based on buoyant plume theory (Morton et al., 1956), coupled with a three-equation melt model (Holland and Jenkins, 1999). The form of the plume equations used here is described in full in Cowton et al. (2015). The initial conditions for the radius and velocity at the subglacial discharge outlet were set using the balance between subglacial channel cross-section, channel discharge and the effective pressure of the overlying ice, as derived by

Slater at al. (2015) based on the work of Schoof (2010). The discharge in the channel was calculated by a surface mass balance model at 6-h intervals through 2017. The ambient temperature and salinity profiles used in the plume model were derived from an average of profiles collected between 0.5 and 3 km distance of the terminus of Kronebreen. The plume equations were then integrated in Python using the lsoda integrator available in the scipy ode package until the plume reached the surface or its neutral buoyancy height. This produced profiles of plume properties, including temperature, salinity and volume fluxes, at 6-h intervals throughout 2017.

The upwelling volume was then calculated as the difference between the initial volume of subglacial discharge and the vertical plume volume flux 1 m below the surface. This assumes that the surface outflow of the plume is ~1 m deep, though altering this depth by 1 or 2 m made very little difference to the results.

2 Supplementary Video

Sup. Video 1 The video file “SI_plumevideo.mp4” shows the upwelling in front of Kronebreen due to the subglacial plume outflow and was recorded on 25 July 2017 during the “Glacier front” expedition. Below a screenshot:

3 Supplementary Figures

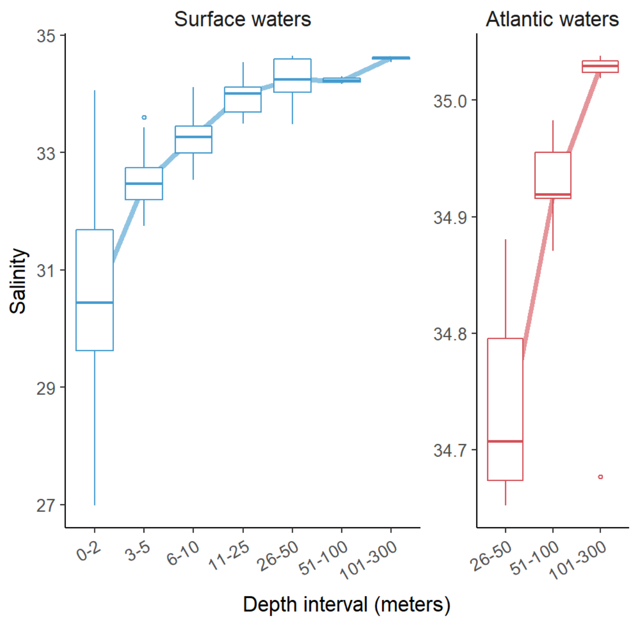

Fig. S1 Salinity-depth relationships for surface (left) and Atlantic (right) waters. The solid line on the background indicates mean values. Note the different scales.

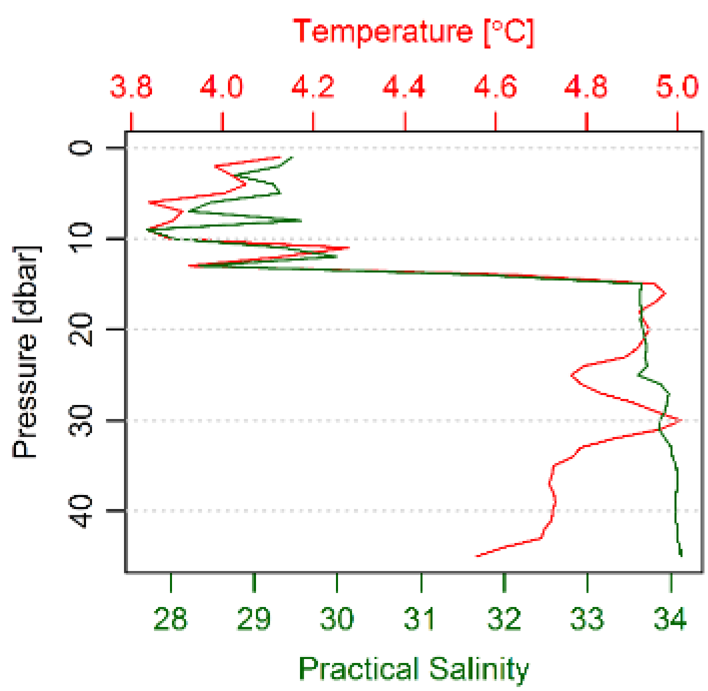

Fig. S2 Temperature and salinity profile at the northernmost station in front of Kronebreen (KpM6, 177 m distance from the glacier front).

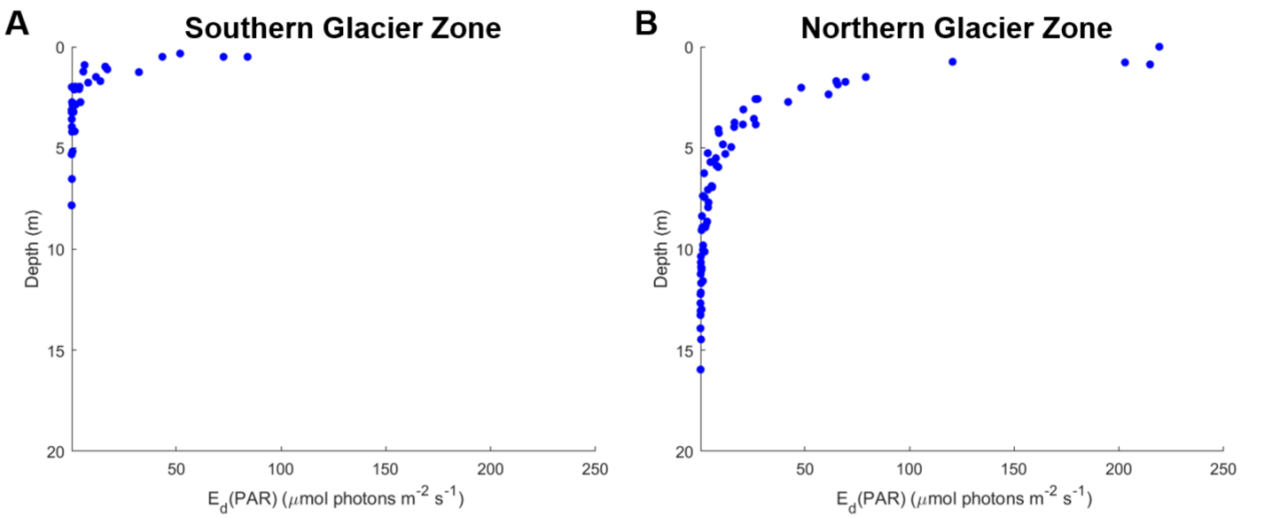

Fig. S3 Vertical profiles of planar downwelling irradiances E_d (PAR) in the Southern Glacier Zone (A) and Northern Glacier Zone (B) (data down to 0.1 µmol photons m^{-2} s^{-1}).

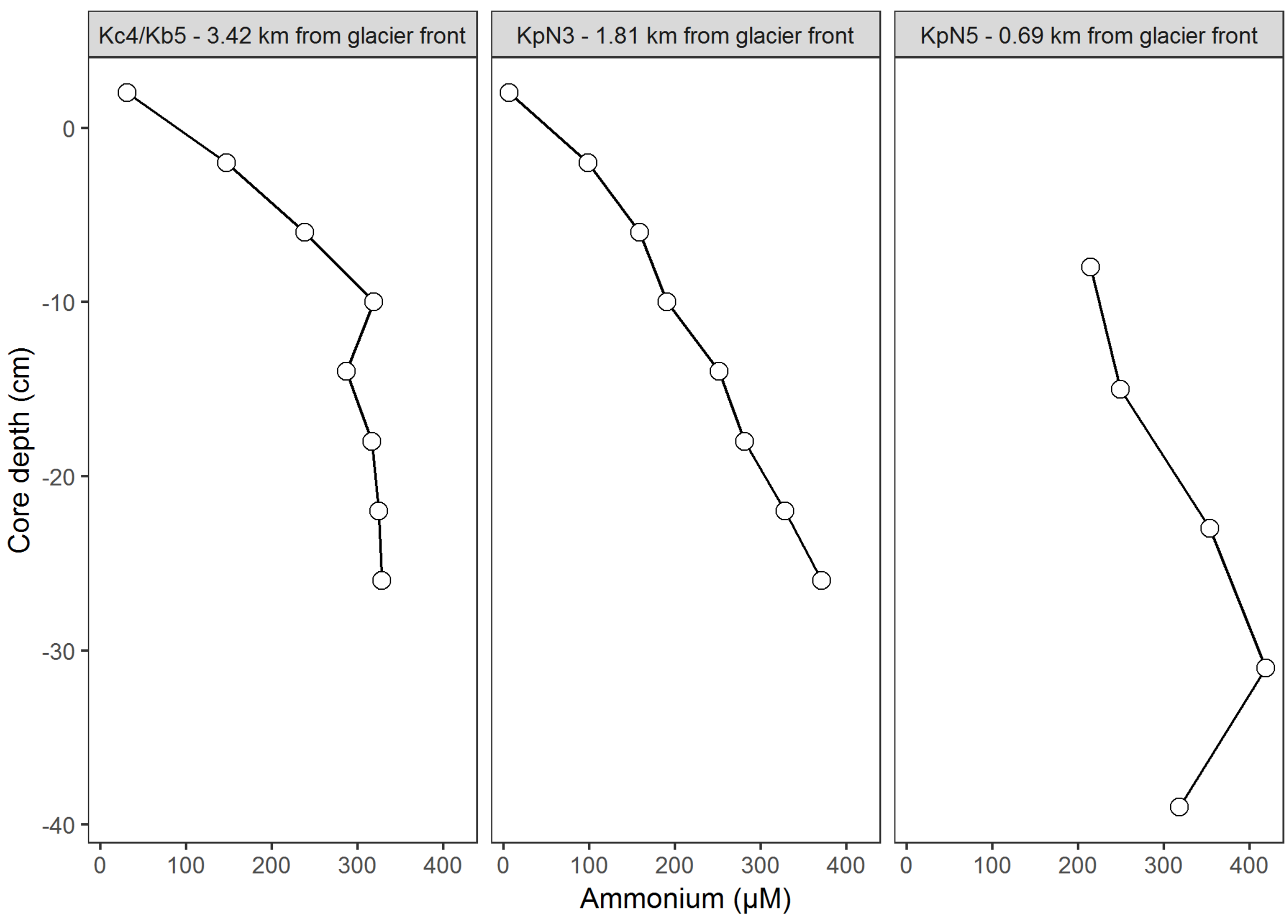

Fig. S4 Ammonium concentrations in the sediment and sediment-water interface at stations Kc4/Kb5, KpN3 and KpN5 (northernmost Kronebreen transect) in the SGZ.

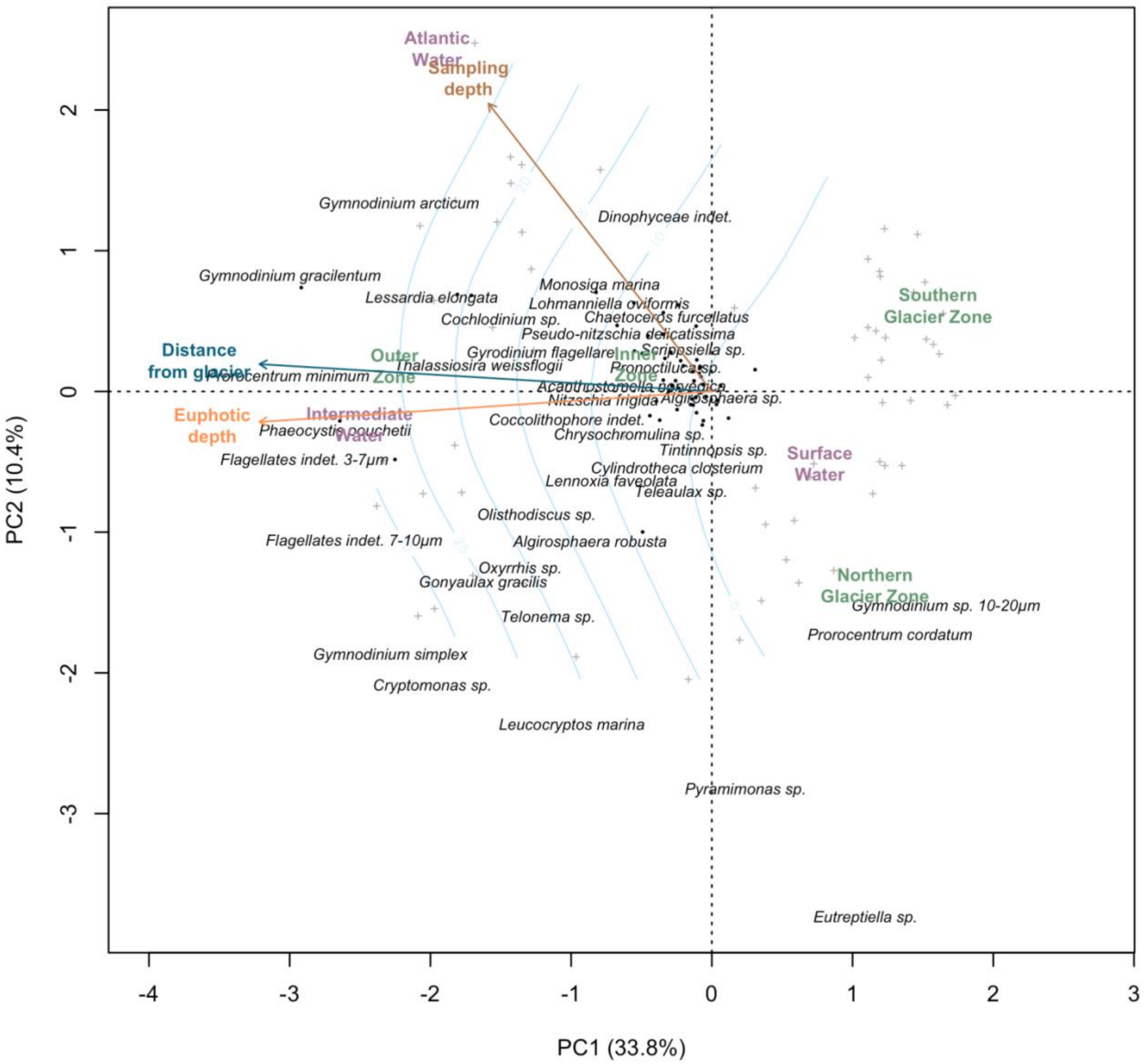

Fig. S5 Principal component analysis (PCA) of logarithmic-transformed phytoplankton abundance matrix with zones (green), sampling depth (brown), water type (purple), euphotic depth (orange), and distance from the glacier (blue) as environmental gradients fitted on the PCA ordination. The environmental variable scores are scaled to make them readable. See Table S3 for actual scores. The blue contour lines indicate nonlinear fit of distance from the glacier. Individual Niskin bottle samples were used as "sites" and are illustrated using grey crosses. Species scores are illustrated using black dots, and most contributing species are presented as labels. Total variance explained by each PCA axis is given in parenthesis in axis labels. Salinity correlated with sampling depth and temperature with distance from the glacier and bottom depth, respectively (Table S3). Consequently, salinity, temperature and bottom depth are not shown in the figure.

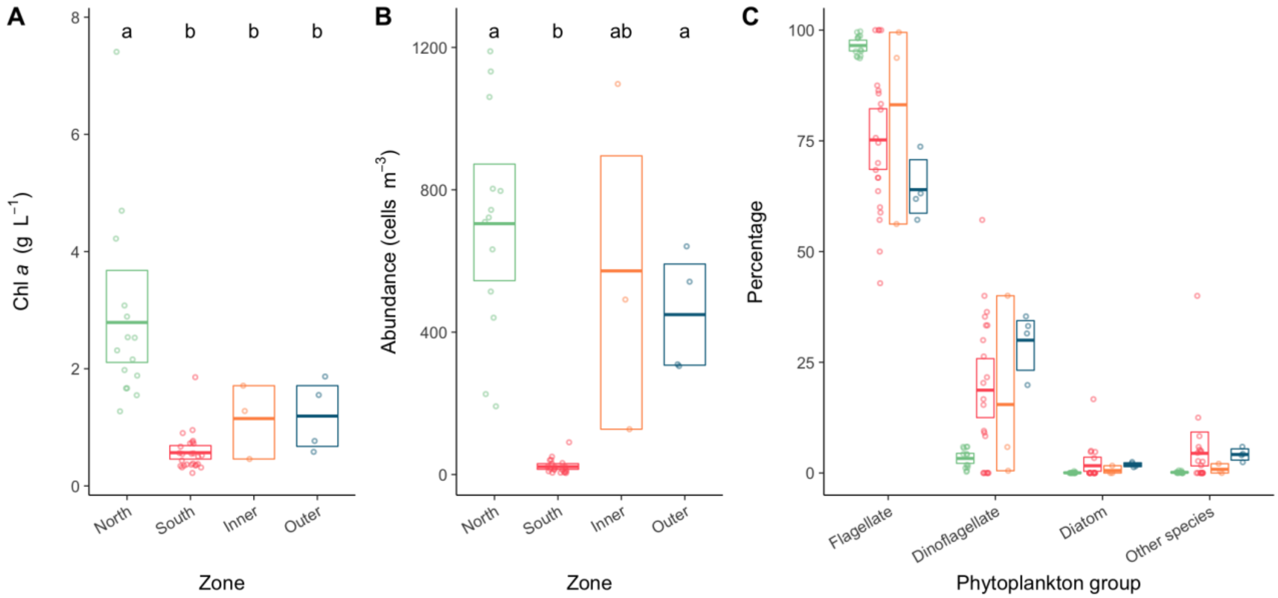

Fig. S6 Chlorophyll *a* (Chl *a*, A), phytoplankton abundance (B) and phytoplankton community composition (C) data used in the study.

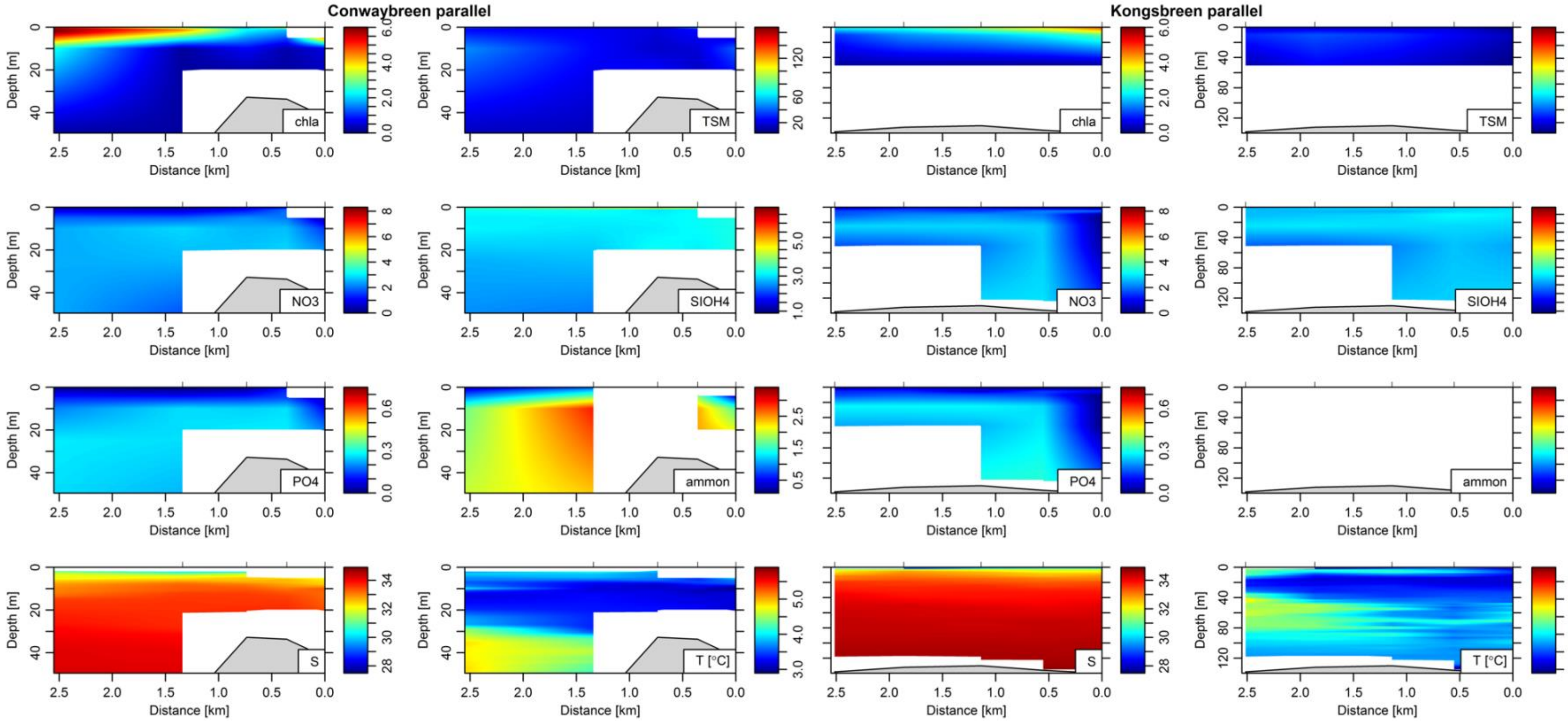

Fig. S7 CTD profiles for Chlorophyll *a* (Chl *a* [mg m^{-3}]), suspended matter (TSM [g m^{-3}]), nitrate (NO_3 [mmol m^{-3}]), silicic acid ($SiOH_4$ [mmol m^{-3}]), phosphate (PO_4 [mmol m^{-3}]), ammonium (ammon [mmol m^{-3}]), salinity (S) and temperature (T [°C]), measured from water samples taken at distinct depths. Profiles in distances to the glacier front of Conwaybreen (left image) and Kongsbreen North (right image).

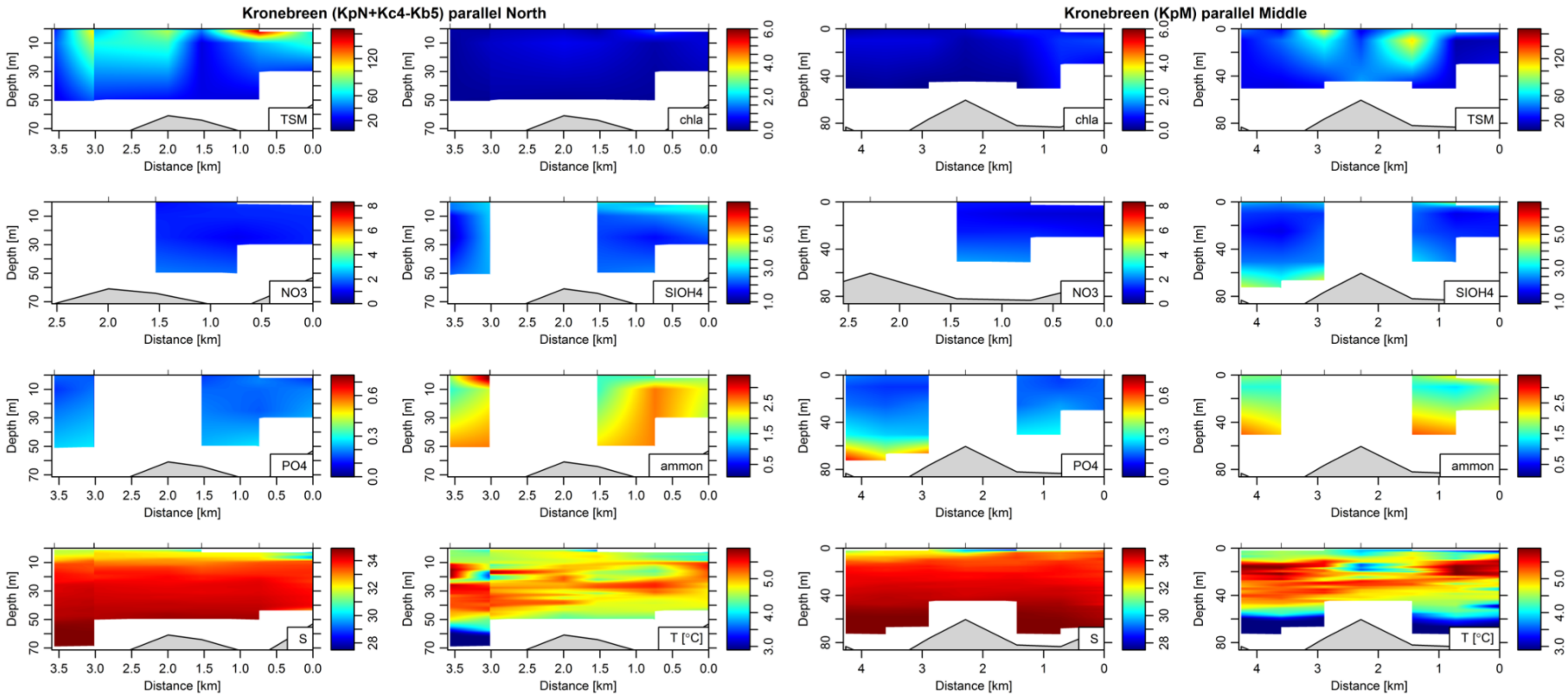

Fig. S8 CTD profiles for Chlorophyll *a* (Chl *a* [mg m^{-3}]), suspended matter (TSM [g m^{-3}]), nitrate (NO_3 [mmol m^{-3}]), silicic acid ($SiOH_4$ [mmol m^{-3}]), phosphate (PO_4 [mmol m^{-3}]), ammonium (ammon [mmol m^{-3}]), salinity (S) and temperature (T [°C]), measured from water samples taken at distinct depths. Profiles in distances to the glacier front of Kronebreen, northern-most transect (KpN, left image) and middle transect (KpM, right image).

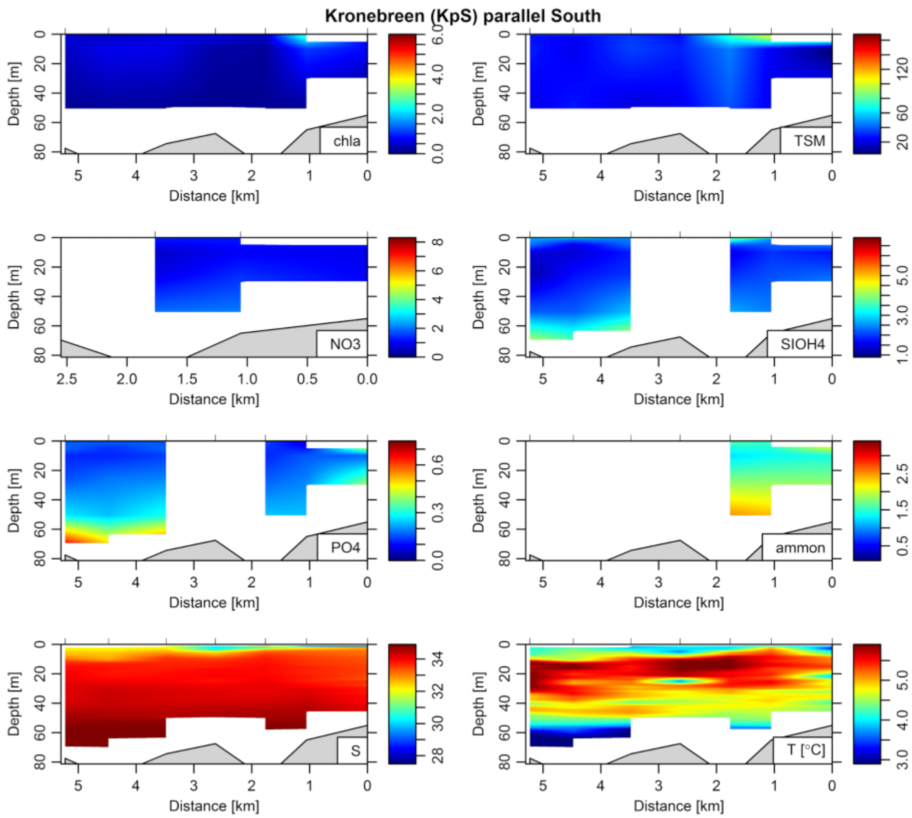

Fig. S9 CTD profiles for Chlorophyll a (Chl a [mg m-3]), suspended matter (TSM [g m^{-3}]), nitrate (NO_3 [mmol m^{-3}]), silicic acid ($SiOH_4$ [mmol m^{-3}]), phosphate (PO_4 [mmol m^{-3}]), ammonium (ammon [mmol m^{-3}]), salinity (S) and temperature (T [°C]), measured from water samples taken at distinct depths. Profiles in distances to the glacier front of Kronebreen, southern most transect (KpS).

4 Supplementary Tables

Table S1 Number of phytoplankton samples taken in the four study regions by depth. Missing value means that no samples were taken at a given depth.

Sampling depth (m)	Outer	Inner	South	North
1				6
5	4	3		4
10	4	1	21	3
25	4	1		
50	4	1		
100	4	1		

Table S2 Taxa encountered in the phytoplankton dataset and their allocation to groups (headers under the Name column). Abundance (cells m^{-3}) and aggregate percentage values are averages of samples from Outer and Inner zone (Fjord) versus Northern and Southern Glacier Zones (Glacier front). Numbers in square brackets indicate minimum and maximum range, while numbers in round brackets represent standard deviation. Empty cells indicate values < 0.005.

	Abundance (cells × 10^3 L^{-1})		Relative abundance	
Name	Fjord	Glacier front	Fjord	Glacier front
Ciliates	1.42 [0-2.44]	0.69 [0-4.16]	0.37 (0.24)	2.18 (4.3)
Acanthostomella norvegica	0.28 [0-0.96]		0.06 (0.08)	
Ciliophora indet. 10-20µm		0.28 [0-4.16]		0.97 (3.73)
Euplotes sp.	0.37 [0-1.36]		0.06 (0.11)	
Leegaardiella sol	0.24 [0-1.55]		0.03 (0.08)	
Lohmanniella oviformis	0.65 [0-1.38]	0.18 [0-1.04]	0.12 (0.12)	0.68 (1.62)
Mesodinium rubrum	0.76 [0-1.9]	0.09 [0-2.13]	0.16 (0.13)	0.15 (0.86)
Parafavella obtusangula	0.04 [0-0.19]		0.02 (0.03)	
Strombidium sp.	0.05 [0-0.13]		0.02 (0.02)	
Tintinnopsis sp.	0.19 [0-1.11]	0.08 [0-1.11]	0.03 (0.04)	0.01 (0.04)
Uronema marinum	0.51 [0-1.66]	0.06 [0-1.1]	0.08 (0.1)	0.37 (2.14)
Diatoms	5.71 [0-13.71]	0.25 [0-1.93]	1.69 (1.41)	1.03 (3.13)
Chaetoceros decipiens	0.8 [0-5.61]		0.17 (0.44)	
Chaetoceros furcellatus	0.64 [0-3.33]		0.08 (0.16)	
Chaetoceros laciniosus	0.16 [0-1.11]		0.02 (0.05)	
Chaetoceros similis	0.24 [0-1.66]		0.03 (0.08)	
Contricibra cf. *weissflogii*		0.03 [0-0.85]		0.05 (0.29)
Cylindrotheca closterium	0.94 [0-3.57]	0.06 [0-1.09]	0.25 (0.35)	0.02 (0.08)
Fragilariopsis cylindrus	1.18 [0-4.2]		0.22 (0.29)	
Fragilariopsis oceanica	0.87 [0-2.91]		0.16 (0.21)	
Lennoxia faveolata	0.94 [0-3.15]		0.14 (0.18)	
Navicula pelagica	0.13 [0-0.93]		0.07 (0.19)	
Navicula sp.	0.13 [0-0.93]		0.03 (0.07)	
Nitzschia frigida	1.01 [0-2.58]		0.18 (0.2)	
Nitzschia promare	0.48 [0-1.95]		0.08 (0.13)	
Pseudo-nitzschia delicatissima	1.71 [0-7.23]	0.05 [0-1.01]	0.29 (0.39)	0.19 (0.89)
Pseudo-nitzschia granii	0.69 [0-2.18]	0.02 [0-0.64]	0.13 (0.2)	0.05 (0.27)

Rhizosolenia hebetata	0.22 [0-1.35]		0.06 (0.12)	
Stenoneis sp.	0.24 [0-1.67]		0.13 (0.35)	
Synedropsis sp.		0.03 [0-0.85]		0.05 (0.29)
Thalassiosira gravida/antarctica	0.95 [0-3.34]	0.04 [0-0.85]	0.33 (0.69)	0.54 (2.86)
Thalassiosira sp.		0.03 [0-1.04]		0.14 (0.82)
Thalassiosira weissflogii	2.71 [0-7.02]		0.6 (0.54)	
Dinoflagellates	90.78 [2.5-191.6]	10.48 [0-43.94]	23.55 (15.17)	12.81 (15.08)
Alexandrium sp.	0.6 [0-1.66]	0.05 [0-0.89]	0.09 (0.12)	0.18 (1.01)
Amphidinium sphenoides	0.3 [0-2.07]		0.06 (0.16)	
Amphidoma acuminata	0.89 [0-3.34]	0.03 [0-1.06]	0.18 (0.26)	
Cochlodinium cf. *pulchellum*	0.24 [0-1.66]		0.03 (0.09)	
Cochlodinium sp.	0.9 [0-2.21]		0.16 (0.18)	
Dinophyceae indet.	3.28 [0-6.91]	0.56 [0-3.4]	0.65 (0.48)	1.32 (3.28)
Dinophysis contracta	0.19 [0-1.32]		0.05 (0.12)	
Dinophysis rotundata	0.03 [0-0.12]	0.02 [0-0.83]	0.01 (0.02)	0.08 (0.44)
Gonyaulax gracilis	3.72 [0-6.43]	0.16 [0-1.11]	0.66 (0.46)	0.12 (0.39)
Gymnodiniales indet. 10-20µm	7.56 [0-14.92]		1.56 (1.11)	
Gymnodiniales indet. 30-40µm	0.16 [0-1.15]		0.02 (0.06)	
Gymnodinium cf. arcticum	3.53 [0-6.78]	0.03 [0-1.04]	0.8 (0.72)	0.14 (0.82)
Gymnodinium galeatum	6.12 [0-9.96]	0.33 [0-3.27]	1.39 (1.15)	0.2 (0.86)
Gymnodinium cf. gracilentum	15.72 [0-32.05]	0.28 [0-4.44]	3.89 (4.08)	0.33 (1.13)
Gymnodinium simplex	31.11 [0.83-124.81]	1.03 [0-8.53]	4.87 (5.68)	1.67 (5.57)
Gymnodinium sp. 10-20µm	1.03 [0-5.55]	2.93 [0-17.26]	0.12 (0.21)	4.14 (7.63)
Gymnodinium sp. 20-30µm		0.26 [0-5.45]		0.04 (0.18)
Gymnodinium wulffii	3.25 [0-6.13]	0.24 [0-4.15]	0.91 (1.16)	0.31 (1.71)
Gyrodinium flagellare	1.32 [0-3.06]		0.35 (0.4)	
Gyrodinium fusiforme	1.07 [0-2.19]	0.33 [0-4.27]	0.24 (0.2)	1.01 (5.71)
Gyrodinium sp.	0.35 [0-1.32]		0.07 (0.13)	
Heterocapsa cf. *niei*	0.14 [0-0.95]		0.02 (0.05)	
Heterocapsa rotundata	1.54 [0-3.71]	0.38 [0-5.45]	0.26 (0.27)	0.05 (0.17)
Katodinium glaucum	0.5 [0-1.32]	0.13 [0-4.27]	0.17 (0.24)	0.02 (0.1)
Lessardia elongata	1.82 [0-3.33]		0.4 (0.32)	
Micracanthodinium claytonii	0.35 [0-1.29]		0.06 (0.07)	
Oxyrrhis sp.	2.77 [0-5.91]	1.02 [0-11.85]	0.63 (0.57)	0.54 (1.29)
Oxytoxum gracile	0.02 [0-0.13]			
Polarella glacialis	0.83 [0-5.79]		0.17 (0.46)	
Pronoctiluca sp.	0.13 [0-0.9]		0.03 (0.07)	
Prorocentrum cordatum	4.28 [0-29.94]	2.59 [0-22.32]	0.39 (1.03)	2.49 (4.26)
Prorocentrum gracile	0.24 [0-1.66]		0.03 (0.08)	
Prorocentrum minimum	16.74 [0-36.37]		3.29 (3.18)	
Protoperidinium brevipes	0.52 [0-1.36]		0.13 (0.22)	
Protoperidinium cerasus	0.14 [0-0.95]		0.02 (0.05)	
Protoperidinium pellucidum	0.7 [0-1.66]	0.03 [0-1.09]	0.17 (0.24)	0.01 (0.03)
Scrippsiella sp.	0.66 [0-1.9]	0.08 [0-1.1]	0.1 (0.12)	0.18 (1.01)
Flagellates	393.65 [71.59-1028.59]	271.34 [2.5-1168.33]	71.87 (18.02)	83.36 (16.99)
Astasia sp.	0.71 [0-3.33]		0.15 (0.31)	
Calliacantha natans	2.19 [0-5.11]		0.67 (0.98)	
Calycomonas sp.	0.5 [0-1.33]		0.1 (0.13)	
Chrysophyceae indet.	9.11 [0-14.08]	0.88 [0-4.16]	2.25 (2.23)	2.9 (5.18)
Commation sp.	0.42 [0-1.58]	0.15 [0-4.27]	0.08 (0.14)	1.15 (5.77)
Cryptomonas sp.	49.63 [2.44-227.23]	0.85 [0-8.93]	6.71 (10.19)	1.37 (4.11)
Dunaliella sp.	0.85 [0-1.84]		0.26 (0.36)	
Eutreptiella sp.	258.14 [21.96-756.14]	230.77 [0-1109.01]	39.35 (28.74)	48.94 (32.88)
Flagellates indet. 3-7µm	31.54 [0-58.57]	1.4 [0-8.99]	6.61 (4.89)	3.54 (8.13)
Flagellates indet. 7-10µm	26.85 [0-48.78]	2.02 [0-14.12]	4.79 (2.56)	2.44 (5.83)
Leucocryptos marina	5.77 [0.83-18.13]	1.04 [0-12.8]	1.1 (0.84)	2.54 (4.66)

Leucocryptos sp.		0.02 [0-0.64]		0.05 (0.27)
Monosiga marina	1.56 [0-3.33]		0.32 (0.24)	
Olisthodiscus sp.	2.1 [0-4.24]	0.42 [0-4.12]	0.48 (0.48)	0.58 (1.46)
Pachysphaera sp.	0.48 [0-3.35]		0.06 (0.16)	
Pyramimonas sp.	51.79 [4.41-184.83]	32.5 [0-536.62]	7.4 (5.14)	17.98 (15.92)
Teleaulax sp.	3.45 [0-20.47]	0.6 [0-4.12]	0.48 (0.96)	1.16 (3.09)
Telonema sp.	3.99 [0-10.43]	0.66 [0-6.54]	0.79 (0.58)	0.71 (2.2)
Prymnesiophytes	11.39 [0-30.16]	0.35 [0-4.16]	2.53 (2.04)	0.62 (3.43)
Algirosphaera robusta	2.12 [0-7.98]		0.4 (0.72)	
Algirosphaera sp.		0.03 [0-0.91]		
Chrysochromulina sp.	1.07 [0-3.11]		0.19 (0.2)	
Coccolithophore indet.	1.82 [0-6.39]	0.09 [0-3.16]	0.31 (0.37)	0.01 (0.07)
Emiliania huxleyi	0.61 [0-2.34]	0.12 [0-4.16]	0.24 (0.43)	0.59 (3.43)
Phaeocystis pouchetii	8.91 [0-24.21]	0.11 [0-2.13]	1.49 (1.31)	0.01 (0.06)
Prymnesiophyceae indet.	0.22 [0-1.55]		0.03 (0.08)	

Table S3 Explanatory variable fit to the unconstrained PCA ordination of logarithm transformed phytoplankton abundance matrix presented in Fig. S8. Type column gives the type of the variable (categorical vs. continuous gradient), R^2 indicates the goodness of fit statistic for fitted linear regression gradients, whereas PC1 and PC2 the principal component coordinates of biplot arrows for continuous variables.

Type	Variable	R^2	PC1	PC2
Categorical	Area	0.53		
	Water type	0.44		
Continuous	Distance from glacier	0.74	-1.00	0.06
	Euphotic depth	0.68	-1.00	-0.07
	Sampling depth	0.61	-0.61	0.79
	Salinity	0.53	-0.63	0.78
	Temperature	0.22	-0.98	-0.18

Table S4 Diffuse attenuation coefficients (K_d (λ)) [m^{-1}] at PAR and selected wavelengths (nm) for the Southern Glacier Zone and Northern Glacier Zone.

Zone	Station	Glacier distance (km)	z1 (m)	z2 (m)	K_d (PAR)	Wavelength (nm)					
						K_d (412)	K_d (443)	K_d (490)	K_d (510)	K_d (555)	K_d (670)
SGZ	Kc1	3.66	1.1	3.2	1.3	2.1	1.9	1.6	1.5	1.2	1.4
	Kc2	3.74	1.2	3.6	1.6	4.1	2.6	2.2	2.1	1.7	1.5
	Kc3	3.76	1.2	3.6	1.6	4.1	2.6	2.2	2.1	1.7	1.5
	Kc4	3.42	0.5	2.9	1.3				5.7	3.6	2.6
	Kc5	3.23	2	3	2.6				7	3.5	2.5
	Kc6	3.04	1.7	2.7	1.1	1.6	1.4	1.2	1.1	1	1.3
	KpN1	3.11	1.5	3.2	2.9				5.8	3.9	2.8
	KpN2	2.89	1.3	3.1	3.1		7	5.8	5.6	4	2.9
	KpN3	1.82	0.9	2.8	4.6						4.2
	KpN5	0.69	0.5	2	4.2			6.7	6.3	5.1	3.7
NGZ	Cc2	2.29	1.7	3.6	0.5	0.7	0.6	0.5	0.5	0.4	0.8
	Cc3	1.98	2.4	3.8	0.7	1.1	1	0.8	0.7	0.6	1
	Cc4	1.86	2.6	4.1	0.7	1	0.9	0.8	0.7	0.6	1.1
	CpN2	1.30	1.7	3.8	0.5	0.6	0.5	0.4	0.4	0.4	0.7
	CpN3	0.67	1.5	2.6	1	0.9	0.8	0.7	0.6	0.6	1
	CpN4	0.38	2	3.1	0.8	1.1	1	0.8	0.7	0.6	1.1

5 Supplementary References

Cowton T., Slater D., Sole A., Goldberg D. and Nienow P. (2015) Modeling the impact of glacial runoff on fjord circulation and submarine melt rate using a new subgrid-scale parameterization for glacial plumes. *J. Geophys. Res. Ocean*, 120(2), 796–812.

Holland, D. M., and A. Jenkins (1999), Modeling thermodynamic ice-ocean interactions at the base of an ice shelf, J. Phys. Oceanogr. 29(8), 1787–1800. doi:10.1175/1520-0485(1999)029<1787:MTIOIA>2.0.CO;2

Morton, B. R., Taylor, G., and Turner, J. S. (1956). Turbulent gravitational convection from maintained and instantaneous sources. *Proc. R. Soc. A Math. Phys. Eng. Sci*. 234, 1–23. doi:10.1098/rspa.1956.0011.

Oksanen, J., Blanchet, F. G., Friendly, M., Kindt, R., Legendre, P., McGlinn, D., et al. (2018). Vegan: Community Ecology Package. Available online at: https://cran.r-project.org/package=vegan

Pramanik, A., Van Pelt, W., Kohler, J., and Schuler, T. V. (2018). Simulating climatic mass balance, seasonal snow development and associated freshwater runoff in the Kongsfjord basin, Svalbard (1980–2016). *J. Glaciol*. 1–14. doi:10.1017/jog.2018.80.

Schoof, C. (2010). Ice-sheet acceleration driven by melt supply variability. *Nature*, 468, 803–806. doi:10.1038/nature09618.

Slater D. A., Nienow P. W., Cowton T. R., Goldberg D. N. and Sole A. J. (2015). Effect of near-terminus subglacial hydrology on tidewater glacier submarine melt rates. *Geophys. Res. Lett*., 42(8), 2861–2868. doi:10.1002/2014GL062494.

Van Pelt, W. J. J., Oerlemans, J., Reijmer, C. H., Pohjola, V. A., Pettersson, R. & Van Angelen, J. H. 2012. Simulating melt, runoff and refreezing on Nordenskiöldbreen, Svalbard, using a coupled snow and energy balance model. *Cryosphere*, 6, 641-659 doi: 10.5194/tc-6-641-2012.

Vihtakari, M. (2017). *PlotSvalbard: PlotSvalbard - plot research data from Svalbard on maps*. R package version 0.1.0. https://mikkovihtakari.github.io/PlotSvalbard/